LJMU Research Online

Gao, Y, Liu, X, Ren, S, Li, Y and Zhang, Y

 Role of Surface Roughness in Surface Energy Calculation of Aggregate Minerals

http://researchonline.ljmu.ac.uk/id/eprint/24146/

Article

For more information please contact researchonline@ljmu.ac.uk

1 **Role of Surface Roughness in Surface Energy Calculation of Aggregate Minerals**
2
3 **Yangming Gao, PhD**
4 [a] Marie Curie Research Fellow
5 Section of Pavement Engineering
6 Department of Structural Engineering
7 Faculty of Civil Engineering & Geosciences
8 Delft University of Technology
9 Delft, The Netherlands, 2628 CN
10 Email: Y.Gao-3@tudelft.nl
11 [b] Senior Lecturer
12 School of Civil Engineering and Built Environment
13 Liverpool John Moores University
14 Liverpool, United Kingdom, L3 3AF
15
16 **Xueyan Liu, PhD**
17 Associate Professor
18 Section of Pavement Engineering
19 Department of Structural Engineering
20 Faculty of Civil Engineering & Geosciences
21 Delft University of Technology
22 Delft, The Netherlands, 2628 CN
23 Email: x.liu@tudelft.nl
24
25 **Shisong Ren**
26 PhD candidate
27 Section of Pavement Engineering
28 Department of Structural Engineering
29 Faculty of Civil Engineering & Geosciences
30 Delft University of Technology
31 Delft, The Netherlands, 2628 CN
32 Email: Shisong.Ren@tudelft.nl
33
34 **Yuanyuan Li, PhD**
35 Lecturer
36 School of Civil Engineering and Architecture
37 Wuhan Institute of Technology
38 Wuhan, China, 430074
39 liyy@wit.edu.cn
40
41 **Yuqing Zhang, PhD**
42 Professor
43 School of Transportation
44 Southeast University
45 Nanjing, China, 211189
46 Email: zhangyuqing@seu.edu.cn
47 *(Corresponding Author)*
48

Y. Gao, X. Liu, S. Ren, Y. Li and Y. Zhang

1 **ABSTRACT**
2 Surface energy is a key material property and can work as a crucial parameter in various mechanical
3 models to predict the moisture sensitivity and fatigue damage of asphalt mixtures. The calculated
4 surface energy values of the aggregate minerals strongly depend on their surface roughness.
5 Therefore, it is very relevant for accurate calculation of surface energy to study the relationship
6 between roughness and surface energy. This study aims to investigate the relationship between
7 surface roughness and surface energy of aggregate minerals. Two minerals, quartz and calcite, were
8 used for this study. The surfaces of the mineral specimens were treated to achieve four levels of
9 roughness. Their surface roughness was described by three roughness parameters. Based on the sessile
10 drop (SD) method, an optical tensiometer with a 3D topography module was employed to measure the
11 contact angle and the surface energy of the minerals with different roughness. The influences of
12 surface roughness on the contact angle and the surface energy were then analyzed. The results showed
13 that the contact angle for both quartz and calcite decreases with the increasing surface roughness
14 when it's less than 90° and increases when it's greater than 90°. Wenzel equation can remove the
15 effect of surface roughness on the contact angles of the minerals. The surface energy of quartz and
16 calcite in the presence of roughness at the microscale would be underestimated when using the
17 measured (apparent) contact angle. The corrected surface energy based on the Wenzel equation must
18 be applied to represent the real surface energy of the minerals.
19 **Keywords:** aggregate minerals, surface roughness, contact angle, surface energy, sessile drop (SD)
20 method.

1   **INTRODUCTION**
2   Aggregates (i.e., rock particles) with diverse mineral compositions are one of the most widely
3   used construction materials. In asphalt pavements, the aggregates are applied to fabricate the asphalt
4   concrete when mixed with bitumen. The weight of the aggregates can be up to around 95% of the
5   whole asphalt concrete. The interfacial adhesion between the aggregates and bitumen plays a critical
6   role in the durability of asphalt pavements. The adhesive deterioration of the aggregates with bitumen
7   would cause severe pavement distresses such as strength degradation (*1; 2*), moisture damage (*3; 4*)
8   and fatigue cracking (*5*).
9   Surface energy of aggregates is a key material property, which can be directly related to
10 moisture sensitivity and fatigue resistance of asphalt concrete through the adhesive bonding between
11 the aggregates and bitumen. It has been widely used as a crucial parameter in thermodynamic and
12 mechanical models to investigate the fundamental failure mechanisms of asphalt concrete. Lytton et
13 al. (*6*) proposed a surface energy-based approach to evaluate the moisture sensitivity of asphalt
14 concrete. In their study, surface energy of aggregates was measured to calculate the adhesive bond
15 strength between the aggregate and bitumen and then predict moisture damage of asphalt concrete.
16 Little and Bhasin (*7*) measured the surface energy of various aggregates and pure minerals to select
17 materials for the optimum moisture performance of asphalt concrete. Recently, many studies (*8-10*)
18 have been conducted to further evaluate the adhesive bond strength and moisture sensitivity of
19 aggregate-bitumen systems based on surface energy of aggregates. In addition to moisture damage,
20 surface energy of aggregates can be used to evaluate the fatigue damage of asphalt concrete. The
21 surface energy of aggregates is an important input of material property in fatigue models according to
22 principles of fracture mechanics. Cheng et al. (*11*) applied surface energy of aggregates to predict the
23 fatigue cracking characteristics of asphalt concrete. In the study, the fatigue model was a function of
24 the surface energy of the aggregates, which was developed based on Schapery's viscoelastic fracture
25 mechanics law. The fatigue performance predicted by surface energy of aggregates agreed well with
26 experimental results. Zhang et al. (*12*) employed viscoelastic Griffith's criterion to develop a fatigue
27 crack initiation model for asphalt concrete under external compressive loads. In their fatigue model,
28 the surface energy of aggregates was an important parameter that influenced the crack initiation in
29 asphalt concrete. Similarly, Luo, Luo and Lytton (*13*) investigated the fatigue crack initiation of
30 asphalt concrete under tensile loads and found that the surface energy of aggregates was directly
31 related to the fatigue crack initiation.
32   The surface energy measurements of aggregates can be performed by using different methods
33 including a universal sorption device (USD) and a sessile drop (SD) device. The USD-based testing
34 method computers the surface energy of aggregates by measuring the spreading pressure of various
35 liquids on the aggregate surface, which is inherently complex and time-consuming. Compared to the
36 USD, the SD device is cheaper and simpler and requires minimal training. It has been extensively
37 used in various fields (e.g., chemical, geology, mining, petroleum, coating, etc.) to investigate wetting
38 and surface energy through direct measurement of contact angles. The SD device directly measures
39 the contact angle of probe liquids on the solid surface to calculate the surface energy and its results
40 are relatively accurate and reliable. The SD method has been applied for the surface energy
41 measurements of aggregates. Little and Bhasin (*7*) used the SD method to measure the surface energy
42 of four aggregates (i.e., limestone, gravel, basalt and granite). It was reported that the surface energy
43 of aggregates depended on the exact mineralogical composition of the aggregate. Koc and Bulut (*14*)
44 further assessed the SD device employed for surface energy measurements of five Oklahoma
45 aggregates. It was recommended that the roughness of aggregate sample surfaces must be minimized
46 and the roughness level should be below 1 micrometer. Moraes, Velasquez and Bahia (*9*) tested the
47 surface energy of two aggregates (i.e., granite and limestone) with the SD device to evaluate the
48 moisture resistance of aggregate-bitumen systems. This study indicated that the different mineral
49 groups present on aggregate surface significantly affected on the measured surface energy of the
50 aggregate. Based on these studies, it was found that the surface energy values for the aggregates
51 exhibited a very broad variation, which could be caused by mineral composition and surface
52 roughness of the aggregates. Chau et al. (*15*) have reported that surface roughness had a significant
53 impact on the contact angle on solid surfaces when they investigated the contact angle and the wetting
54 behavior of solid particles in flotation. Therefore, a study is urgently needed to understand the role of
55 surface roughness in the surface energy calculation of aggregate minerals in asphalt concrete.

1   The objective of this study is to investigate the influence of surface roughness on the surface
2   energy calculation of the aggregate minerals to develop a quantitative relationship between surface
3   roughness and surface energy. Two minerals, i.e., quartz and calcite, were prepared and their surfaces
4   were treated to obtain four levels of roughness. A novel laboratory test that can combine surface
5   roughness and contact angle measurements was designed by using an optical tensiometer with a 3D
6   topography module. The contact angle measurement was conducted on the exactly same sample areas
7   as tested by the topography measurement. The surface energy of the minerals with different surface
8   roughness was then determined based on a sessile drop (SD) method. Furthermore, the relationship
9   between surface roughness and surface energy of the minerals was developed by analyzing the effect
10 of surface roughness on the surface energy calculation.
11
12 **MATERIALS AND METHODS**
13 **Materials**
14   Two types of pure minerals (i.e., quartz and calcite) obtained from Ward's Natural Science
15 were tested in this study to evaluate their contact angles and surface energy by Sessile Drop (SD)
16 method. Quartz (SiO_2) and calcite ($CaCO_3$) are the two most common mineralogical compositions of
17 the aggregates that are widely used in asphalt concrete. For example, quartz exists in granite with a
18 high percentage, while limestone consists mainly of calcite. The mineral specimens ranged in size
19 from 2×2 to 4×4 cm^2 for the cross-section and from 1 to 4 cm for the thickness. Contact angle
20 measurements can be conducted for the specimen sizes.
21
22 **Preparation of Mineral Specimens With Different Surface Roughness**
23   A protocol was developed for the specimen preparation to directly measure contact angles on
24 mineral specimens using the SD method. The specimen surfaces must be relatively flat and clean for
25 the accurate measurement of contact angles. The specimens were firstly polished by hand using the
26 fine (1000 grit) sandpapers with the abrasive material of silicon carbide to obtain a smooth surface.
27 After that, the smooth surfaces were treated using different sandpapers with number 320, 150, 120,
28 and 80 grits. Through controlling the polishing time (2 min), four types of specimen surfaces (No. 1,
29 2, 3 and 4) with a certain roughness can be created for contact angle measurements. Surface
30 roughness measurements in the next section indicate that different levels of roughness can be
31 successfully created by following the polishing method. All the specimens were then cleaned in
32 boiling distilled water and put inside an oven at a temperature of 105 °C for 24 h. The specimens were
33 finally allowed to cool to room temperature. **Figure 1** presents the specimen surfaces with a certain
34 surface roughness for (a) quartz and (b) calcite.
35

36
37   **(a)**   **(b)**
38 **Figure 1 Specimen surfaces with a certain surface roughness for (a) quartz and (b) calcite**
39
40 **Surface Roughness Measurement**
41   The surface roughness of mineral specimens was measured using a 3D topography module of
42 an optical tensiometer from Biolin Scientific. Some topography-specific parameters were firstly set in
43 the recipe when the topography module was connected. The autofocus and autobrightness functions
44 were selected to find the focus and brightness level for each sample automatically. The value of
45 repetitions was set as 5 to perform the measurements in a single run. The results were the averages of

all the measurements. The thickness of sample was written in the recipe. After that, the sample was placed on the sample stage and the test area of the sample was chosen. The sample stage was then automatically moved below the topography camera to start the measurements. Once the measurements have been performed, the results of surface roughness can be obtained including the optical image and topography parameters.

Contact Angle Measurement

Contact angle measurements were conducted using Sessile Drop (SD) method in which contact angle was directly measured by capturing an image of the probe liquid on the solid sample surface. The SD method has been widely used in different disciplines for contact angle measurements of a variety of materials (*14; 16; 17*). According to the Good-van Oss-Chaudhury theory (*18*), determining surface energy using the Sessile Drop method requires that appropriate probe liquids are selected: (a) the surface energy components of probe liquids must be known and (b) their surface energy components are significantly different with regard to their polarities. Therefore, Glycol (EG), Formamide (F) and Distilled Water (W) that have been frequently used in the literature were selected as the probe liquids in this study for contact angle measurements. Their surface energy components are summarised in **Table 1**.

TABLE 1 Surface energy components of probe liquids used in this study (mJ/m^2)

Liquids	Γ	Γ^{LW}	Γ^+	Γ^-
Ethylene Glycol (EG)	48.00	29.00	1.92	47.00
Formamide (F)	58.00	39.00	2.28	39.60
Distilled Water (W)	72.80	21.80	25.50	25.50

The optical tensiometer from Biolin Scientific was employed to perform the contact angle measurements at room temperature (20 °C). The Sessile Drop (SD) device was first calibrated prior to measurements. The mineral samples were then put on the sample stage between the light source and the camera of the device. A small drop of the probe liquid (2 µl of volume) was dispensed from the dispenser on the sample surface. An image of the drop was finally captured by the camera. The captured image can be automatically analyzed by the device to obtain the left and right angles between the baseline and the edge of the drop. Three measurements were carried out for each probe liquid to analyze the variability of the results. The average value for all the measurements was reported as the contact angle between the sample surface and the probe liquid.

The optical tensiometer used in this study is able to combine contact angle and surface roughness measurements in the SD experiment. The topography measurement was conducted for surface roughness evaluation firstly, followed by the contact angle measurement. The contact angle measurement was performed on the exactly same sample areas (1.1 mm × 1.4 mm) as tested by the topography measurement. Thus, the contact angle on the mineral sample with a certain surface roughness can be obtained using the optical tensiometer.

RESULTS AND DISCUSSION
Surface Roughness Evaluation

Surface roughness can be characterized by a set of roughness parameters. **Table 2** presents some common roughness parameters that have been defined to describe surface topography (*19-22*). S_p and S_v are the maximum height of the peaks and the maximum depth of the valleys, respectively. R_z gives the absolute height (the peak to valley value). S_a defines an arithmetic average height of the surface. These amplitude parameters characterize the amplitude of the topography features but cannot reveal their spatial distribution. Instead, the root mean square roughness (S_q) is a statistical moment of the spatial distribution of height that gives the standard deviation of height. The root mean square roughness has been the most widely used roughness parameter due to providing a better roughness description. S_{dr} is a ratio between the interfacial and projected areas, which quantifies the additional surface area contributed by the roughness. The surface area ratio is particularly useful in wettability characterization as it can be utilised to calculate the roughness ratio (*r*) that will be discussed in the next section.

1
2 **TABLE 2 Roughness parameters defined to describe surface topography**

| Parameters	Description	Mathematical definition	Equation No.
S_p	Maximum height of peaks	$S_p = MAX\left(\eta_p\right)$	(1)
S_v	Maximum depth of valleys	$S_v = MIN\left(\eta_v\right)$	(2)
S_z	Absolute height (Maximum height of the surface)	$S_z = \left(\left|S_p\right| + \left|S_v\right|\right)$	(3)
S_a	Arithmetic average roughness	$S_a = \dfrac{1}{MN}\sum_{j=1}^{N}\sum_{i=1}^{M}\left|\eta\left(x_i, y_j\right)\right|$	(4)
S_q	Root mean square roughness	$S_q = \sqrt{\dfrac{1}{MN}\sum_{j=1}^{N}\sum_{i=1}^{M}\eta^2\left(x_i, y_j\right)}$	(5)
S_{dr}	Surface area ratio	$S_{dr} = \dfrac{A_{textured} - A_{cross}}{A_{cross}} \times 100\%$	(6)

3
4   The surface roughness of mineral specimens was examined using the topography module of
5 the optical tensiometer. The digital 2D and 3D surface representations of a sample are illustrated in
6 **Figure 2**. The optical image of each surface with a certain roughness can be obtained by the
7 measurements. **Figure 3** shows the digital surface representations with four different roughness levels
8 of quartz and calcite, respectively. These optical images can clearly describe the surface topography.
9 It should be noted that the size of mineral surface morphology ranges from –30 µm to +30 µm. Based
10 on the topography data, the roughness parameters were estimated using the own software of the
11 instrument. Three roughness parameters, i.e., S_q, S_a, and S_{dr} of all eight mineral surfaces were
12 summarised in **Table 3**. It is seen that the created four mineral surfaces for quartz and calcite exhibit
13 significant differences in the roughness with the ranking of No. 1 < No. 2 < No. 3 < No. 4.
14 Therefore, the surface roughness of quartz and calcite at the microscale can be well measured and
15 characterized using the optical tensiometer.
16
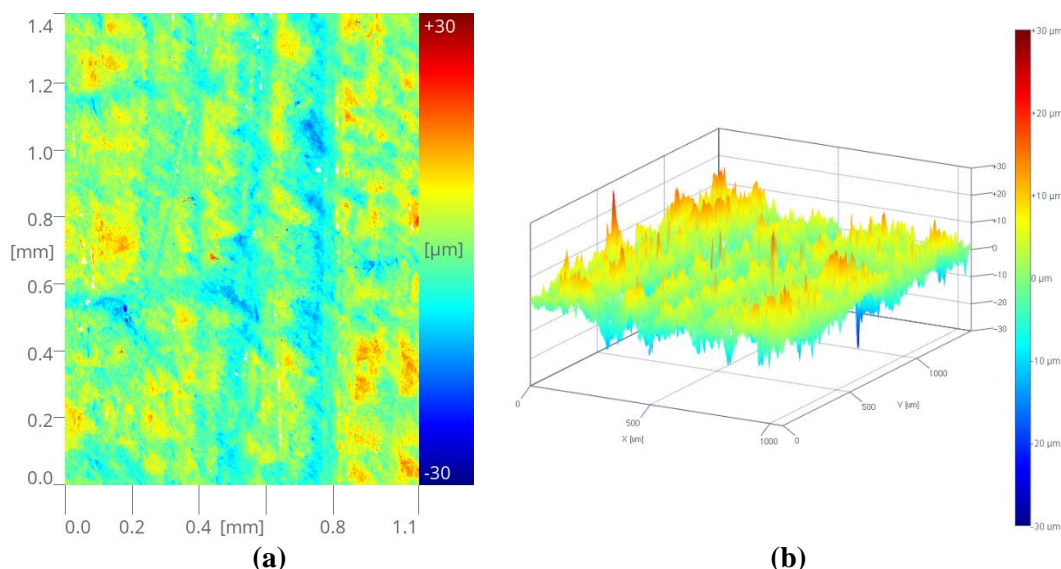
17
18   **(a)**   **(b)**
19 **Figure 2 Typical optical images for surface roughness measurement of a mineral specimen. (a)**
20 **Topography 2D and (b) Topography 3D**
21
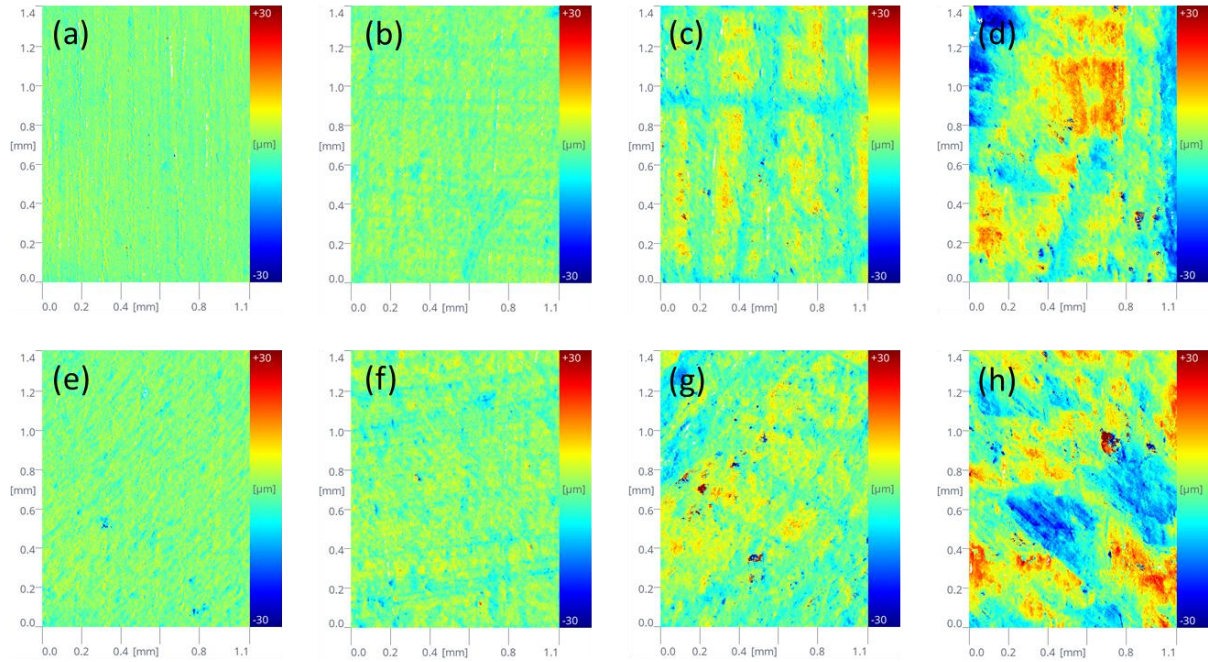
1
2 **Figure 3 Topography 2D images of mineral surfaces with different roughness. (a) quartz No. 1,**
3 **(b) quartz No. 2, (c) quartz No. 3, (d) quartz No. 4, (e) calcite No. 1, (f) calcite No. 2, (g) calcite**
4 **No. 3, and (h) calcite No. 4**
5
6 **TABLE 3 Roughness parameters of different mineral surfaces**

Mineral surfaces	Quartz			Calcite		
	Sq (μm)	Sa (μm)	Sdr (%)	Sq (μm)	Sa (μm)	Sdr (%)
No. 1	2.060	1.516	30.490	3.270	2.393	37.457
No. 2	2.673	2.049	32.737	3.117	2.239	50.382
No. 3	4.866	3.796	42.698	5.358	4.020	62.062
No. 4	6.820	5.191	69.257	8.194	6.289	85.474

7
8 **Effect of Surface Roughness on Contact Angle**
9 A liquid drop can spread on a solid surface up to cover a certain area due to the
10 intermolecular interactions between the solid and the liquid. The wetting interfacial behaviour is
11 usually improved by optimizing the wettability that is defined as the affinity of a solid surface with
12 respect to a given liquid. To characterize the wettability of a solid surface, the contact angle
13 constructed between three phases, i.e., liquid, solid and gas is usually used as an important parameter
14 in wetting processing, as shown in **Figure 4**.
15
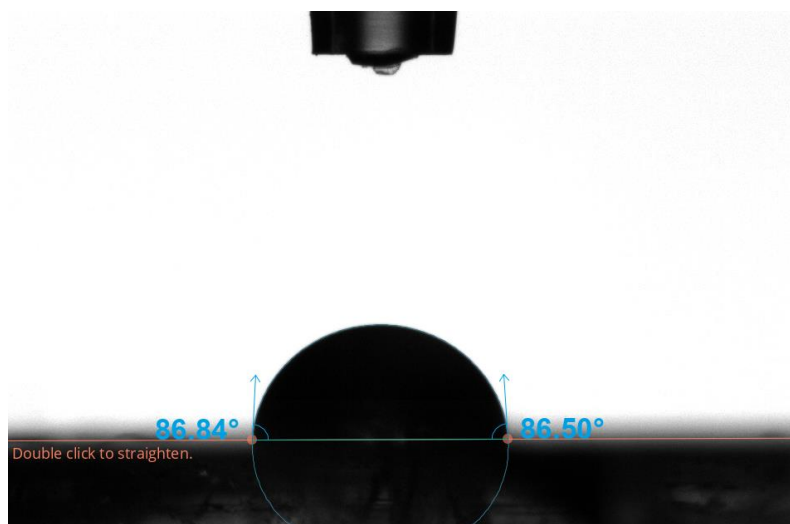
1
2
3 **Figure 4 A typical contact angle between probe liquid and mineral surface**
4
5   **Figure 5** shows the contact angles of three probe liquids i.e., ethylene glycol (EG),
6 formamide (F) and distilled water (W) on the quartz and calcite surfaces with different roughness. It
7 can be seen that the standard deviation (shown by a red error bar) for contact angle measurements of
8 each probe liquid is very low, which indicates that the variability between each measurement is within
9 an acceptable limit and the results are repeatable.
10   It is found from **Figure 5** that for all three probe liquids the contact angles are different on
11 four surfaces with different roughness. The contact angles for ethylene glycol and formamide on both
12 the quartz and calcite surfaces are smaller than 90°, as shown in **Figures 5(a)**, **(b)**, **(d)** and **(e)**. The
13 contact angles decrease with the increase of the roughness described by S_{dr}, which means that the
14 surface roughness reduces the contact angles of ethylene glycol and formamide. However, for distilled
15 water, the contact angles are larger than 90°, see **Figures 5(c)** and **(f)**. Surface No. 4 with the largest
16 roughness has the largest contact angles. The surface roughness causes an increase of the contact
17 angles of distilled water. Thus, it is concluded for both quartz and calcite that the contact angle
18 decreases with growing surface roughness when it's less than 90° and increases when it's greater than
19 90°. This finding is consistent with the previous studies (*23; 24*) that reported the effect of surface
20 roughness on the contact angles for polymer and dental implant surfaces.
21

22
23   **(a)**   **(d)**
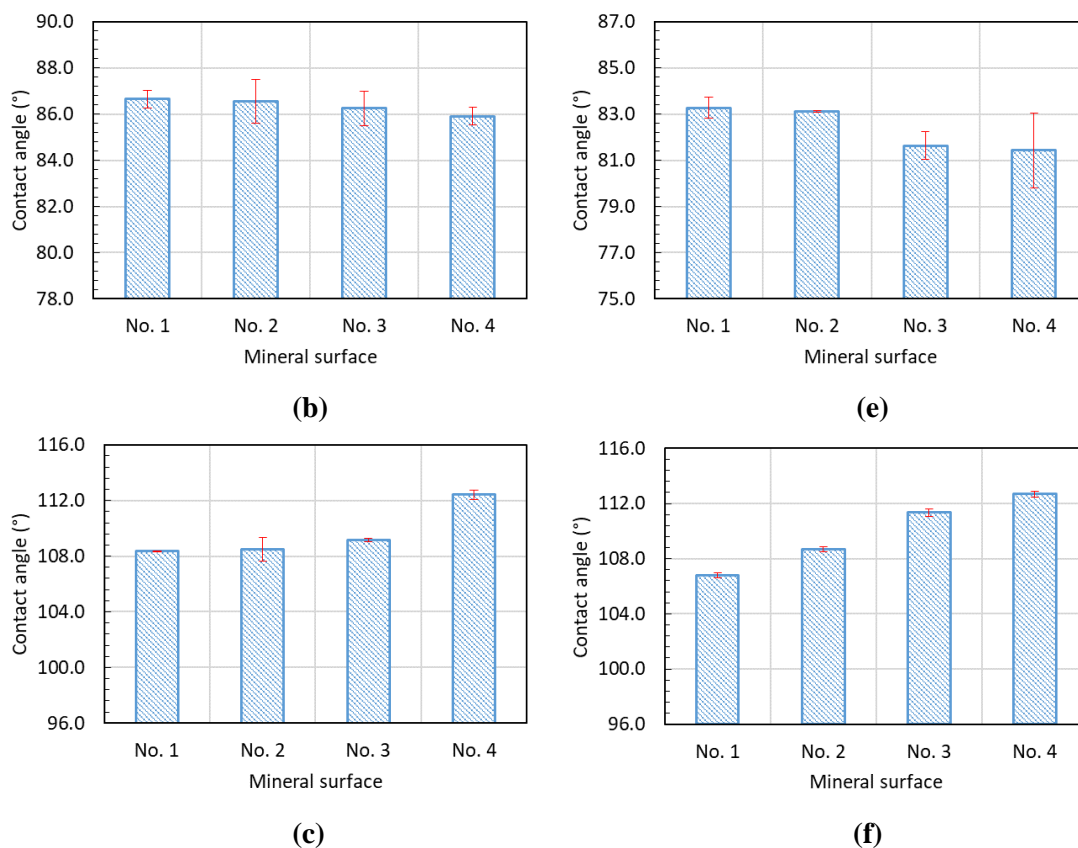
(b)

(e)

(c)

(f)
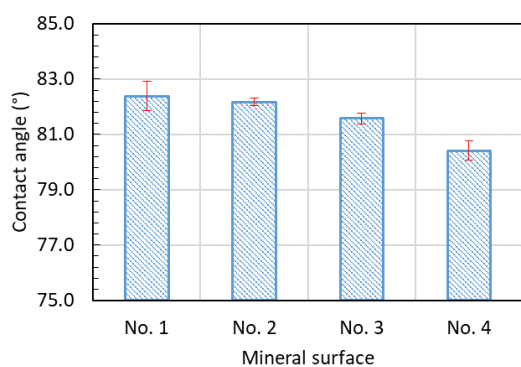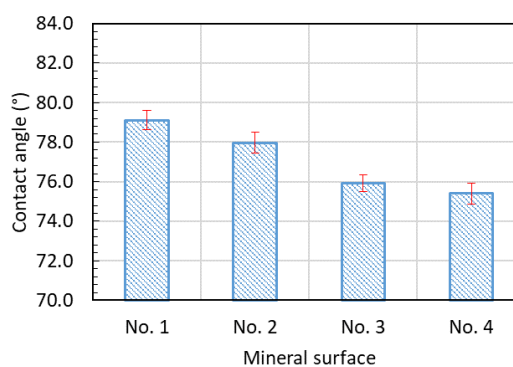
Figure 5 Contact angles of three probe liquids on mineral surfaces with different roughness. (a) quartz-EG, (b) quartz-F, (c) quartz-W, (d) calcite-EG, (e) calcite-F, and (f) calcite-W

Figure 6 presents the contact angles of the liquid on the solid surfaces. The contact angle shown in **Figure 6(a)** on a smooth surface is defined as Young contact angle. The Young equation requires that the surface is unattainable smooth (ideal). However, most real surfaces are non-ideal and do not meet the condition. On a real (rough) surface, the contact angle shown in **Figure 6(b)** is the measured (apparent) contact angle. The Young and measured contact angles can deviate substantially from each other due to the surface roughness. To calculate the surface energy of the solid, the Young contact angle must be used. The relationship between the contact angles and the surface roughness has been already defined by Wenzel (*25*), as expressed in **Equation 7**. It is assumed in **Equation 7** that the liquid completely penetrates into the roughness grooves of the solid surface, as shown in **Figure 6(b)**.

$$\cos \theta_m = r \cos \theta_Y \tag{7}$$

$$r = 1 + S_{dr}/100 \tag{8}$$

where θ_Y is the Young contact angle, θ_m is the measured (apparent) contact angle, and r is the roughness ratio that can be calculated from the surface area ratio S_{dr} described in **Table 2**. It can be seen from **Equation 8** that the roughness ratio $r = 1$ is for a smooth surface and $r > 1$ for a rough one.
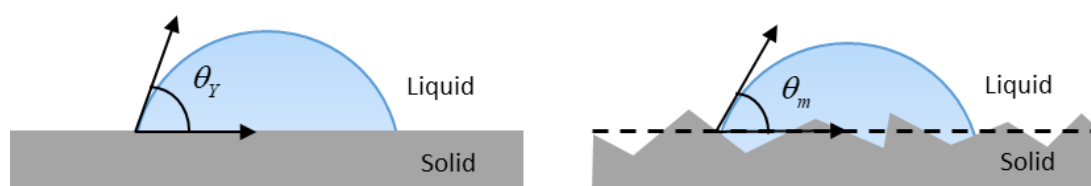
1   **(a)**   **(b)**

2 **Figure 6 Definition of contact angles. (a) Contact angle on ideal surface is called Young contact**
3 **angle, (b) Apparent or measured contact angle on rough (Wenzel) surface**
4
5   The Wenzel equation (**Equation 7**) is used in this study to correct the measured contact angle
6 based on the roughness ratio, which is valid as the drop size of the liquid is sufficiently large
7 compared to the roughness scale. **Figure 7** shows the corrected contact angles of three probe liquids
8 on the quartz and calcite surfaces with different roughness. To compare the contact angle values
9 before and after correction, the uncorrected contact angles are also presented in **Figure 7**. It can be
10 found from **Figure 7** that for all three probe liquids the corrected contact angle values are nearly the
11 same on four surfaces with different roughness, which represent the real contact angle without the
12 effect of surface roughness. The corrected contact angles of ethylene glycol and formamide are larger
13 than their uncorrected contact angles, see **Figures 7(a)**, **(b)**, **(d)** and **(e)**. However, the corrected
14 contact angles of distilled water are smaller than their uncorrected contact angles, as shown in
15 **Figures 7(e)** and **(f)**. The difference between the uncorrected and corrected contact angles increases
16 with the increase of the roughness. Their difference is largest on Surface No. 4 due to the largest
17 roughness. In conclusion, the contact angles corrected by the Wenzel equation can remove the effect
18 of surface roughness and thus represent the real contact angles on the quartz and calcite surfaces. The
19 Wenzel corrected contact angles have been used to investigate cell adhesion to biomaterial surfaces
20 (*22*) and the wettability of paper sheets (*26*).
21

22
23   **(a)**   **(d)**

24
25   **(b)**   **(e)**
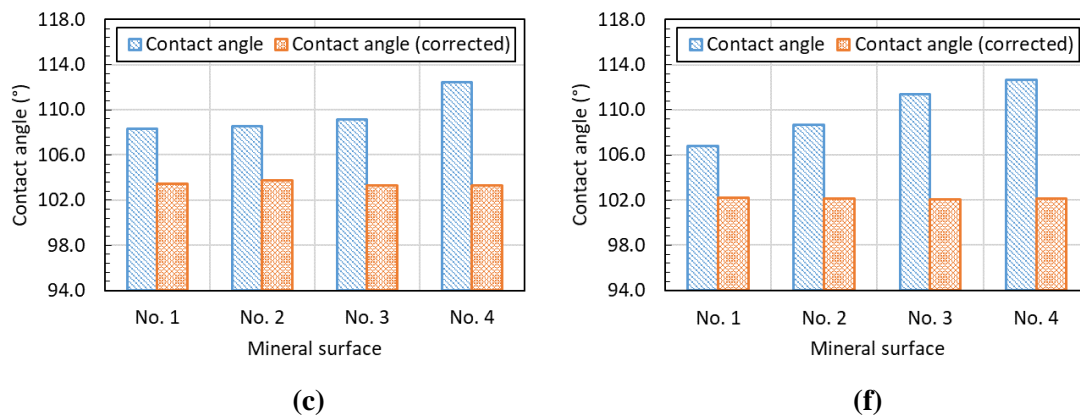
(c)   (f)
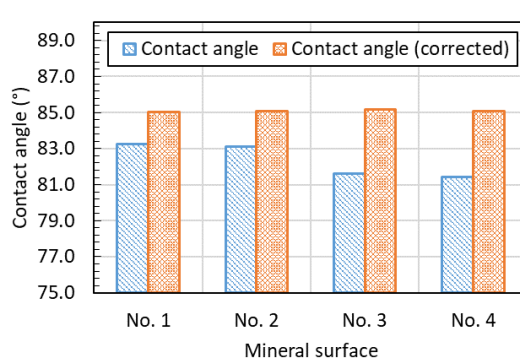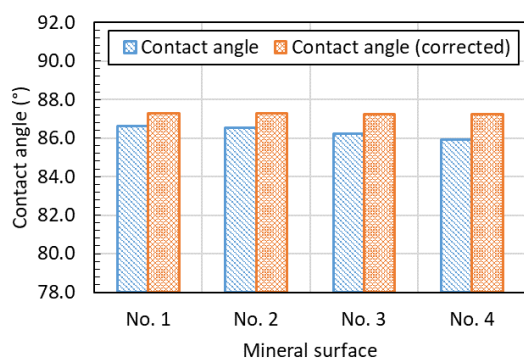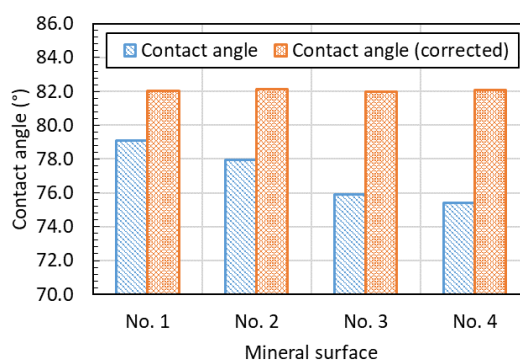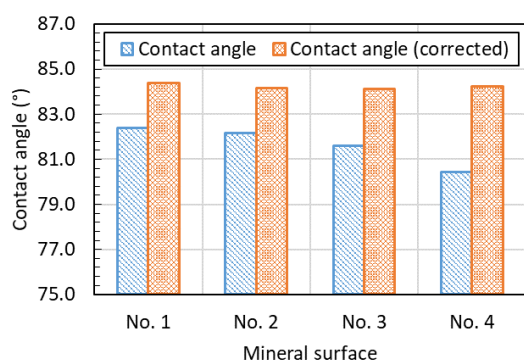
Figure 7 Uncorrected and corrected contact angles on mineral surfaces with different roughness. (a) quartz-EG, (b) quartz-F, (c) quartz-W, (d) calcite-EG, (e) calcite-F, and (f) calcite-W

Surface Energy Calculation

The contact angle between the liquid and solid is intimately related to their surface energy. Young (*27*) defined the relationship between surface energy and contact angle, as shown in **Equation 9**. **Figure 8** presents the contact angle between a liquid drop and a solid surface with three variables of Young's Equation. It is important to notice that the contact angle is the Young contact angle. The Young equation assumes that the solid surface is homogenous and topographically smooth (*28*). A surface that meets the assumption is referred to as an ideal surface, as shown in **Figure 6(a)**. However, most real (practical) surfaces do not meet the requirement. The contact angle on such non-ideal surfaces is referred to as the apparent contact angle, as shown in **Figure 6(b)**. In order to accurately calculate surface energy based on the measured contact angles on a rough surface, the Young contact angles must be firstly estimated through **Equation 7**, as pointed out by Morra, Della Volpe and Siboni (*29*).

$$\gamma_S = \gamma_{SL} + \gamma_L \cos\theta_Y \tag{9}$$

where γ_S is the surface energy of solid (*S*), and γ_L is the surface energy of liquid (*L*), and γ_{SL} is the interfacial energy between the solid and the liquid.
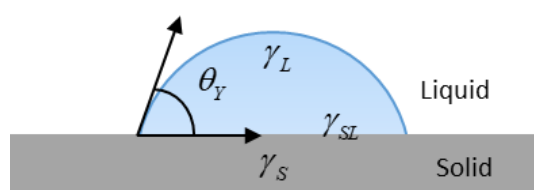

Figure 8 Contact angle between a liquid drop and a solid surface

Based on the Young equation (**Equation 9**), the contact angle is widely used to determine the surface energy of the solid, which is a preferred method since it allows the analysis of the material surface properties at its exact surface (*18*). Surface energy is defined as the work required to form a unit area of new surface in the bulk of a material. According to the Good-van Oss-Chaudhury (GvOC) theory (i.e., the acid-base theory) (*30*), the surface energy (γ) consists of the non-polar component (Lifshitz-van der Waals (LW), γ^{LW}) and the polar component (Lewis acid-base (AB), γ^{AB}), as described in **Equation 10**. The polar component is further composed of the Lewis acid component (γ^+) and the Lewis base component (γ^-), as shown in **Equation 11**.

$$\gamma = \gamma^{LW} + \gamma^{AB} \tag{10}$$

11

$$\gamma^{AB} = 2\sqrt{\gamma^+\gamma^-} \tag{11}$$

Similarly, the interfacial energy (γ_{SL}) between the solid and the liquid shown in **Equation 9** can be divided into the Lifshitz-van der Waals component (γ_{SL}^{LW}) and the Lewis acid-base component (γ_{SL}^{AB}), as expressed in **Equation 12**. In the interfacial energy, the Lifshitz-van der Waals component (γ_{SL}^{LW}) is given by the Good-Girifalco-Fowkes combining rule (*31*) shown in **Equation 13** and the acid-base component (γ_{SL}^{AB}) is obtained by **Equation 14** (*32*).

$$\gamma_{SL} = \gamma_{SL}^{LW} + \gamma_{SL}^{AB} \tag{12}$$

$$\gamma_{SL}^{LW} = \left(\sqrt{\gamma_S^{LW}} - \sqrt{\gamma_L^{LW}}\right)^2 \tag{13}$$

$$\gamma_{SL}^{AB} = 2\left(\sqrt{\gamma_S^+} - \sqrt{\gamma_L^+}\right)\left(\sqrt{\gamma_S^-} - \sqrt{\gamma_L^-}\right) \tag{14}$$

where γ_S^{LW}, γ_S^+, γ_S^- are the Lifshitz-van der Waals, Lewis acid, Lewis base components of a solid, respectively; and γ_L^{LW}, γ_L^+, γ_L^- are the Lifshitz-van der Waals, Lewis acid, Lewis base components of a liquid, respectively. Based on **Equations 10**, **11**, **13** and **14**, **Equation 12** is rewritten as

$$\gamma_{SL} = \gamma_S + \gamma_L - 2\left(\sqrt{\gamma_S^{LW}\gamma_L^{LW}} + \sqrt{\gamma_S^+\gamma_L^-} + \sqrt{\gamma_S^-\gamma_L^+}\right) \tag{15}$$

By combining **Equations 9** and **15,** the Young-Dupre equation is obtained, as given in **Equation 16**.

$$\left(1 + \cos\theta_Y\right)\gamma_L = 2\left(\sqrt{\gamma_S^{LW}\gamma_L^{LW}} + \sqrt{\gamma_S^+\gamma_L^-} + \sqrt{\gamma_S^-\gamma_L^+}\right) \tag{16}$$

The Young-Dupre equation (**Equation 16**) is employed to determine the surface energy components (i.e., γ_S^{LW}, γ_S^+ and γ_S^-) of a solid once the contact angle measurements are conducted on the solid by using three different probe liquids with the known surface energy characteristics (i.e., γ_L^{LW}, γ_L^+ and γ_L^-). After these surface energy components of the solid were obtained, its surface energy can be determined using **Equations 10** and **11**. **Table 4** shows the uncorrected and corrected surface energy of the tested minerals with different roughness. The uncorrected surface energy was obtained from the measured (apparent) contact angle (θ_Y), while the corrected surface energy was determined by the Young contact angle (θ_m) estimated based on Wenzel equation (**Equation 7**).

TABLE 4 Surface energy of quartz and calcite with different roughness (mJ/m²)

Mineral	Surface energy (mJ/m²)			
	Quartz		Calcite	
	Uncorrected	Corrected	Uncorrected	Corrected
No. 1	19.19	20.47	22.39	22.19
No. 2	19.02	20.03	20.20	22.27
No. 3	18.67	19.95	20.06	21.57
No. 4	16.97	20.24	19.18	22.19

1
2 **Effect of Surface Roughness on Surface Energy Calculation**
3   The uncorrected and corrected surface energy of quartz and calcite with different roughness
4 are illustrated in **Figure 9**. The effect of surface roughness on the surface energy calculation of the
5 minerals is analyzed to reveal the relationship between surface roughness and surface energy
6 calculation. The results of **Figure 9** show that the surface roughness has a significant influence on the
7 uncorrected surface energy for both quartz and calcite. It can be observed that the calculated values of
8 the uncorrected surface energy decrease with an increase in the surface roughness. This finding agrees
9 well with the previous study (*33*) showing the surface energy of the hydrophobic material decreased
10 as the surface roughness increased. Thus, it can be concluded that the surface energy is
11 underestimated by the measured (apparent) contact angle in the presence of roughness on the mineral
12 surfaces at the microscale.
13   However, it is also seen from **Figure 9** that the values of the corrected surface energy are
14 nearly the same for different surface roughness, which implies that the corrected surface energy has
15 successfully removed the effect of the surface roughness. It is realised that surface energy is a
16 fundamental material property that does not change with an increase/decrease in surface roughness.
17 Therefore, the corrected surface energy based on the Wenzel equation must be applied to represent the
18 real surface energy of materials.
19   As shown in **Figure 9**, calcite has a larger value of the corrected surface energy than quartz,
20 which indicates that the calcite can lead to better interfacial adhesion with bitumen. This finding can
21 be supported by the surface energy data of aggregates in the literature (*9*) that reported that the surface
22 energy (31.3 mJ/m^2) of limestone with calcite as its main component was larger than that (19.3
23 mJ/m^2) of granite (in which quartz is the major component). It is noted that there is a slight
24 discrepancy between the measured values and the literature data. This is because that granite and
25 limestone also contain a small amount of other minerals such as albite, feldspar and dolomite.
26   It is also noted from **Figure 9** that the corrected surface energy values of quartz and calcite
27 are close to each other. Surface energy values for mineral materials reported in the literature (*34*)
28 show a very broad variation. The variation can be caused by many factors such as chemical
29 composition, crystal structure and surface morphology. Therefore, it is possible (acceptable) that the
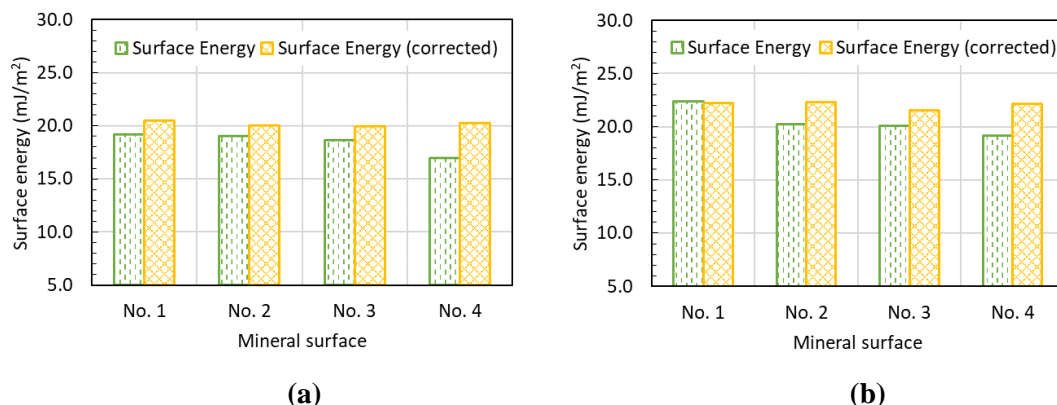30 similar surface energy values are obtained for both quartz and calcite.
31

33   **(a)**   **(b)**
34 **Figure 9 Uncorrected and corrected surface energy of minerals with different surface**
35 **roughness. (a) quartz (b) calcite**
36
37 **CONCLUSIONS AND RECOMMENDATION**
38   In this study, the relationship between surface roughness and surface energy of the aggregate
39 minerals was investigated using an optical tensiometer with a 3D topography module. The quartz and
40 calcite specimens with four levels of roughness were prepared and their surface roughness was
41 evaluated using three roughness parameters. A sessile drop (SD) method was used to measure the
42 contact angle and the surface energy of the minerals with different roughness. The effect of surface
43 roughness on the contact angle and the surface energy were then analyzed. The main conclusions can
44 be drawn from this study:

- The contact angle for both quartz and calcite decreases with growing surface roughness when it's less than 90° and increases when it's greater than 90°.
- The contact angle corrected by the Wenzel equation can remove the effect of surface roughness and thus represent the Young contact angle on the quartz and calcite surfaces.
- The surface energy of quartz and calcite would be underestimated if using the measured (apparent) contact angle in the presence of roughness on the mineral surfaces at the microscale.
- The corrected surface energy based on the Wenzel equation must be applied to represent the real surface energy of quartz and calcite.

In this study, the traditional sessile drop (SD) method was improved through the developed quantitative relationship between surface roughness and surface energy and the novel laboratory test method that can combine topography and contact angle measurements. In future studies, more minerals will be tested to determine the real surface energy of aggregates composed of various minerals. Furthermore, the corrected surface energy will be used to evaluate the adhesion and debonding behaviours of the aggregates with bitumen and to screen appropriate aggregates that can improve the durability of asphalt mixtures.

AUTHOR CONTRIBUTIONS

The authors confirm contribution to the paper as follows: study conception and design: Y. Zhang; data collection: Y. Gao; analysis and interpretation of results: Y. Gao, X. Liu, S. Ren, Y. Zhang, and Y. Li; draft manuscript preparation: Y. Gao. All authors reviewed the results and approved the final version of the manuscript.

REFERENCES

[1] Gao, Y., M. Dong, L. Li, L. Wang, and Z. Sun. Interface effects on the creep characteristics of asphalt concrete. *Construction and Building Materials,* Vol. 96, 2015, pp. 591-598.

[2] Dong, M.-s., Y.-m. Gao, L.-l. Li, L.-n. Wang, and Z.-b. Sun. Viscoelastic micromechanical model for dynamic modulus prediction of asphalt concrete with interface effects. *Journal of Central South University,* Vol. 23, No. 4, 2016, pp. 926-933.

[3] Gao, Y., Y. Zhang, F. Gu, T. Xu, and H. Wang. Impact of minerals and water on bitumen-mineral adhesion and debonding behaviours using molecular dynamics simulations. *Construction and Building Materials,* Vol. 171, 2018, pp. 214-222.

[4] Gao, Y., Y. Zhang, Y. Yang, J. Zhang, and F. Gu. Molecular dynamics investigation of interfacial adhesion between oxidised bitumen and mineral surfaces. *Applied Surface Science,* Vol. 479, 2019, pp. 449-462.

[5] Lytton, R. L., Y. Zhang, F. Gu, and X. Luo. Characteristics of damaged asphalt mixtures in tension and compression. *International Journal of Pavement Engineering,* Vol. 19, No. 3, 2018, pp. 292-306.

[6] Lytton, R. L., E. A. Masad, C. Zollinger, R. Bulut, and D. N. Little. Measurements of surface energy and its relationship to moisture damage.In, 2005.

[7] Little, D. N., and A. Bhasin. Using surface energy measurements to select materials for asphalt pavement.In, 2006.

[8] Grenfell, J., A. Apeagyei, and G. Airey. Moisture damage assessment using surface energy, bitumen stripping and the SATS moisture conditioning procedure. *International Journal of Pavement Engineering,* Vol. 16, No. 5, 2015, pp. 411-431.

[9] Moraes, R., R. Velasquez, and H. Bahia. Using bond strength and surface energy to estimate moisture resistance of asphalt-aggregate systems. *Construction and Building Materials,* Vol. 130, 2017, pp. 156-170.

[10] Zaidi, S. B. A., G. D. Airey, J. Grenfell, R. M. Alfaqawi, I. Ahmed, N. Ahmad, and M. Haynes. Moisture susceptibility of hydrated lime modified mastics using adhesion test methods and surface free energy techniques. *International Journal of Pavement Engineering,* Vol. 22, No. 7, 2021, pp. 829-841.

[11] Cheng, D., D. N. Little, R. L. Lytton, and J. C. Holste. Surface energy measurement of asphalt and its application to predicting fatigue and healing in asphalt mixtures. *Transportation research record,* Vol. 1810, No. 1, 2002, pp. 44-53.

[12] Zhang, Y., X. Luo, R. Luo, and R. L. Lytton. Crack initiation in asphalt mixtures under external compressive loads. *Construction and Building Materials,* Vol. 72, 2014, pp. 94-103.

[13] Luo, X., R. Luo, and R. L. Lytton. Energy-based crack initiation criterion for viscoelastoplastic materials with distributed cracks. *Journal of Engineering Mechanics,* Vol. 141, No. 2, 2014, p. 04014114.

[14] Koc, M., and R. Bulut. Assessment of a sessile drop device and a new testing approach measuring contact angles on aggregates and asphalt binders. *Journal of Materials in Civil Engineering,* Vol. 26, No. 3, 2014, pp. 391-398.

[15] Chau, T., W. Bruckard, P. Koh, and A. Nguyen. A review of factors that affect contact angle and implications for flotation practice. *Advances in colloid and interface science,* Vol. 150, No. 2, 2009, pp. 106-115.

[16] Puri, V., A. K. Dantuluri, M. Kumar, N. Karar, and A. K. Bansal. Wettability and surface chemistry of crystalline and amorphous forms of a poorly water soluble drug. *European journal of pharmaceutical sciences,* Vol. 40, No. 2, 2010, pp. 84-93.

[17] Gao, Y., L. Li, and Y. Zhang. Modelling crack initiation in bituminous binders under a rotational shear fatigue load. *International Journal of Fatigue,* Vol. 139, 2020, p. 105738.

[18] Van Oss, C. J. Use of the combined Lifshitz–van der Waals and Lewis acid–base approaches in determining the apolar and polar contributions to surface and interfacial tensions and free energies. *Journal of adhesion science and technology,* Vol. 16, No. 6, 2002, pp. 669-677.

[19] Blunt, L., and X. Jiang. *Advanced techniques for assessment surface topography: development of a basis for 3D surface texture standards" surfstand".* Elsevier, 2003.

[20] Gadelmawla, E., M. M. Koura, T. M. Maksoud, I. M. Elewa, and H. Soliman. Roughness parameters. *Journal of materials processing technology,* Vol. 123, No. 1, 2002, pp. 133-145.

[21] Ramón-Torregrosa, P., M. Rodríguez-Valverde, A. Amirfazli, and M. Cabrerizo-Vílchez. Factors affecting the measurement of roughness factor of surfaces and its implications for wetting studies. *J Colloids and Surfaces A: Physicochemical and Engineering Aspects,* Vol. 323, No. 1-3, 2008, pp. 83-93.

[22] Rosales-Leal, J. I., M. A. Rodríguez-Valverde, G. Mazzaglia, P. J. Ramón-Torregrosa, L. Díaz-Rodríguez, O. García-Martínez, M. Vallecillo-Capilla, C. Ruiz, and M. J. C. Cabrerizo-Vílchez. Effect of roughness, wettability and morphology of engineered titanium surfaces on osteoblast-like cell adhesion. *J Colloids and Surfaces A: Physicochemical and Engineering Aspects,* Vol. 365, No. 1-3, 2010, pp. 222-229.

[23] Morra, M., E. Occhiello, and F. Garbassi. Knowledge about polymer surfaces from contact angle measurements. *Advances in colloid and interface science,* Vol. 32, No. 1, 1990, pp. 79-116.

[24] Bathomarco, R., G. Solorzano, C. Elias, and R. Prioli. Atomic force microscopy analysis of different surface treatments of Ti dental implant surfaces. *Applied Surface Science,* Vol. 233, No. 1-4, 2004, pp. 29-34.

[25] Wenzel, R. N. Resistance of solid surfaces to wetting by water. *Industrial & Engineering Chemistry,* Vol. 28, No. 8, 1936, pp. 988-994.

[26] Moutinho, I., M. Figueiredo, and P. Ferreira. Evaluating the surface energy of laboratory-made paper sheets by contact angle measurements. *Tappi Journal*, No. 6, 2007, pp. 26-32.

[27] Young, T. An essay on the cohesion of fluids. *Philosophical transactions of the royal society of London*, No. 95, 1805, pp. 65-87.

[28] Kwok, D. Y., and A. W. Neumann. Contact angle measurement and contact angle interpretation. *J Advances in colloid and interface science,* Vol. 81, No. 3, 1999, pp. 167-249.

[29] Morra, M., C. Della Volpe, and S. Siboni. Comment to the paper: Enhancing surface free energy and hydrophilicity through chemical modification of microstructured titanium implant surfaces, by F. Rupp, L. Scheideler, N. Olshanska, M. de Wild, M. Wieland, J. Geis-Gerstorfer. *Journal of biomedical materials research. Part A,* Vol. 79, No. 3, 2006, pp. 752-757.

[30] van Oss, C. J., M. Chaudhury, and R. J. Good. Monopolar surfaces. *Advances in colloid and interface science,* Vol. 28, 1987, pp. 35-64.

[31] Good, R. J., and L. Girifalco. A theory for estimation of surface and interfacial energies. III. Estimation of surface energies of solids from contact angle data. *The Journal of Physical Chemistry,* Vol. 64, No. 5, 1960, pp. 561-565.

[32] Van Oss, C., R. Good, and M. Chaudhury. Additive and nonadditive surface tension components and the interpretation of contact angles. *Langmuir,* Vol. 4, No. 4, 1988, pp. 884-891.

[33] Wang, X., and Q. Zhang. Role of surface roughness in the wettability, surface energy and flotation kinetics of calcite. *Powder Technology,* Vol. 371, 2020, pp. 55-63.

[34] Sauerer, B., M. Stukan, W. Abdallah, M. H. Derkani, M. Fedorov, J. Buiting, and Z. J. Zhang. Quantifying mineral surface energy by scanning force microscopy. *Journal of colloid and interface science,* Vol. 472, 2016, pp. 237-246.